

Stochastic model error in the LANS-alpha and NS-alpha deconvolution models of turbulence

Eric Olson*

June 23, 2015

Abstract

This paper reports on a computational study of the model error in the LANS-alpha and NS-alpha deconvolution models of homogeneous isotropic turbulence. The focus is on how well the model error may be characterized by a stochastic force. Computations are also performed for a new turbulence model obtained as a rescaled limit of the deconvolution model. The technique used is to plug a solution obtained from direct numerical simulation of the incompressible Navier–Stokes equations into the competing turbulence models and to then compute the time evolution of the resulting residual. All computations have been done in two dimensions rather than three for convenience and efficiency. When the effective averaging length scale in any of the models is $\alpha_0 = 0.01$ the time evolution of the root-mean-squared residual error grows as \sqrt{t} . This growth rate is consistent with the hypothesis that the model error may be characterized by a stochastic force. When $\alpha_0 = 0.20$ the residual error grows linearly. Linear growth suggests that the model error possesses a systematic bias which dominates the stochastic terms. Finally, for $\alpha_0 = 0.04$ the LANS-alpha model possessed systematic bias; however, for this value of α_0 the higher-order alpha models that were tested did not.

1 Introduction

Consider two dynamical systems

$$\frac{du}{dt} = \mathcal{F}(u) \quad \text{and} \quad \frac{dv}{dt} = \tilde{\mathcal{F}}(v)$$

on a Hilbert space V with norm $\|\cdot\|$. Suppose the evolution of u is given by exact dynamics and the evolution of v according to some approximate dynamics. Define the model error of the approximate dynamics as the residual R obtained by plugging the exact solution u into the equation governing v . Thus,

$$dR = du - \tilde{\mathcal{F}}(u)dt = (\mathcal{F}(u) - \tilde{\mathcal{F}}(u))dt \quad (1)$$

*Department of Mathematics and Statistics, University of Nevada, Reno, NV 89557, USA.
email: ejolson@unr.edu

where by convention we take $R(0) = 0$. In their analysis of the 4DVAR data assimilation algorithm for the two-dimensional incompressible Navier–Stokes equations, Hoang, Law and Stuart [16] assume that $R = W$ where W is a spatially-correlated and temporally-white Gaussian process and use (1) as a definition for the approximate dynamics $\tilde{\mathcal{F}}$. Under these assumptions, they proceed to show that the inverse problem of finding the posterior distribution of W is a continuous function of noisy observations of the velocity field. In this work we consider the case when the exact dynamics are given the Navier–Stokes equations and the approximate dynamics $\tilde{\mathcal{F}}$ are given by the LANS-alpha model, the NS-alpha deconvolution model of turbulence and a new rescaled limit of the deconvolution model which has an exponentially small consistency error. Our focus is on whether, to what extent, and under what conditions do the actual residuals R obtained through numeric computation for each of these turbulence models behave as spatially-correlated and temporally-white Gaussian processes.

The LANS-alpha model of turbulence is given by the equations

$$\begin{aligned} \frac{\partial v}{\partial t} + (\bar{v} \cdot \nabla)v + v_j \nabla \bar{v}_j &= \nu \Delta v - \nabla p + f, \\ \nabla \cdot \bar{v} &= 0 \quad \text{where} \quad v = (1 - \alpha^2 \Delta)\bar{v}. \end{aligned} \tag{2}$$

Here v is the Eulerian velocity field, \bar{v} is the average velocity field, α is the averaging length scale, ν is the kinematic viscosity, p is the physical pressure and f is a body force. Note that setting $\alpha = 0$ yields the standard Navier–Stokes equations. These equations, originally called the viscous Camassa–Holm equations, were introduced as a closure for the Reynolds averaged Navier–Stokes equations by Chen, Foias, Holm, Olson, Titi and Wynne in 1998 through a series of papers [3, 4, 5]. At the same time, numerical simulations by Chen, Holm, Margolin and Zhang [6] concluded that the LANS-alpha model also functions as an effective subgrid-scale model. Connections to the theory of global attractors and homogeneous isotropic turbulence and global attractors appear in [12].

Note that equations (2) can be derived as the Euler-Poincaré equations of an averaged Lagrangian to which a viscous term, obtained by identifying the momentum in the physical derivation, has been added. This derivation further assumes that the turbulence is homogeneous and isotropic. A body of theoretical and numerical literature on the LANS- α model exists—see [2, 7, 9, 15, 16, 17, 19, 20, 21] and references therein—that, among other things, explores the dependency on α and the limit when $\alpha \rightarrow 0$, relaxes the homogeneity and isotropy assumptions, studies boundary conditions and boundary layers, and treats other physical systems. In summary, the LANS-alpha model is a well-studied turbulence model that is suitable for further study here.

The NS-alpha deconvolution model of turbulence is structurally the same as the LANS-alpha model, except that the derivation allows for the more general filtering relationship between v and \bar{v} given by

$$\bar{v} = D_N(I - \alpha^2 \Delta)^{-1}v \tag{3}$$

where D_N is the N -th order van Cittert approximate deconvolution operator

$$D_N = \sum_{n=0}^N (1 - (1 - \alpha^2 \Delta)^{-1})^n.$$

Note that setting $N = 0$ yields the LANS-alpha model and setting $\alpha = 0$ again yields the incompressible Navier–Stokes equations. This model was introduced by Rebiholz [23] as a helicity correction to higher-order Leray-alpha models. This model and the related alpha-beta models have been the subject of recent numerical work by Kim, Neda, Rebiholz and Fried [18] and others. As this model is closely related to the LANS-alpha model we include it in our study.

In this paper we also study the limit turbulence model obtained by identifying the effective averaging length scale $\alpha_0 = \alpha/\sqrt{N+1}$ in the NS-alpha deconvolution model and then taking $N \rightarrow \infty$ while holding α_0 constant. This results in a new turbulence model with an exponential smoothing filter given by

$$\bar{v} = \left\{ 1 - \exp\left(-\frac{\Delta^{-1}}{\alpha_0^2}\right) \right\} v$$

with the same structure as LANS-alpha and NS-alpha deconvolution models. For convenience of terminology in the remainder of this paper, we will refer to this limit turbulence model as the *exponential-alpha model*.

Since the dynamics of the turbulence models considered here are deterministic, the model error represented by the residual R is also deterministic. To better understand our computations, we first recall what happens when the model error is actually equal to a stochastic force and further what happens when it contains a systematic bias. Suppose $\tilde{\mathcal{F}}(u)dt = \mathcal{F}(u)dt - dW$ where W is a V -valued Q -Brownian motion. Let Ξ be the underlying probability space. For each $\xi \in \Xi$ we obtain a residual realized by the sample path $R(t) = W(t; \xi)$. Thus,

$$\mathbf{E}[\|R(t)\|^2] = \text{Tr} [\text{Cov}(R(t))] = t \text{Tr} Q.$$

If the model error also contains a systematic bias, then $dR = F_b dt + dW$ where $F_b \in V$ is the bias. In this case,

$$\mathbf{E}[\|R(t)\|^2] = t^2 \|F_b\|^2 + t \text{Tr} Q. \tag{4}$$

Note that the root-mean-squared residual error $\mathcal{E}_{\text{rms}}(t) = \mathbf{E}[\|R(t)\|^2]^{1/2}$ grows as \sqrt{t} in the stochastic case and linearly when there is systematic bias.

Returning now to the project at hand, let \mathcal{F} represent the dynamics of the two-dimensional incompressible Navier–Stokes equations and $\tilde{\mathcal{F}}$ be the two-dimensional version of one of the alpha turbulence models described above. Note that the residual R depends on the solution u to the exact dynamics, which in turn, depends on the initial condition u_0 . As we are studying fully developed turbulence that arises from long-term evolution, it is reasonable to suppose u_0 lies on the global attractor \mathcal{A} determined by the exact dynamics. Thus, for each $u_0 \in \mathcal{A}$ we obtain a corresponding residual $R(t; u_0)$. Heuristically identifying

the parameter $\xi \in \Xi$ in the stochastic case with the parameter $u_0 \in \mathcal{A}$ in the deterministic case, we define the root-mean-square residual error used in our computational study by means of the ensemble average

$$\mathcal{E}_{\text{rms}}(t) = \langle \|R(t)\|^2 \rangle^{1/2} = \left\{ \int_{\mathcal{A}} \|R(t; u_0)\|^2 d\mu(u_0) \right\}^{1/2} \quad (5)$$

where μ is a probability measure on \mathcal{A} . We are now able to state our main result: *If α_0 is sufficiently small, then numerical computations show $\mathcal{E}_{\text{rms}}(t)$ grows as \sqrt{t} ; however, if α_0 is too large, then $\mathcal{E}_{\text{rms}}(t)$ grows linearly in time.*

This paper is organized as follows: Section 2 explores the relation between α and N in the NS-alpha deconvolution model to show that the effective averaging length scale α_0 depends on N as $\alpha_0 = \alpha/\sqrt{N+1}$. We then derive the exponential alpha model by taking the limit $N \rightarrow \infty$ while holding α_0 fixed. Section 3 describes the numerical methods used to compute the solution u of the two-dimensional incompressible Navier–Stokes equations that will be plugged into the turbulence models to compute the residual error. In Lemma 1 we show for small enough time steps that the resulting discrete dynamical system possesses a global attractor. Section 4 presents our computational results including our main result on the growth rate of $\mathcal{E}_{\text{rms}}(t)$. The paper ends by summarizing our conclusions and stating some plans for future work.

2 The Effective Averaging Length Scale

In this section we identify the effective averaging length scale in the NS-alpha deconvolution model as $\alpha_0 = \alpha/\sqrt{N+1}$ and then use this identification to derive the exponential-alpha model as the limit $N \rightarrow \infty$ holding α_0 constant.

We consider the effects of the smoothing filter (3) on regular 2π -periodic functions with zero spatial average in Fourier space. Similar results could be obtained in more general settings, however, since our computations will be made for 2π -periodic domains, it is easiest to work in that setting from the beginning. Henceforth, write the functions v and \bar{v} in terms of Fourier series as

$$v(x, t) = \sum_{k \in \mathbf{Z}^2 \setminus \{0\}} v_k(t) e^{ik \cdot x} \quad \text{and} \quad \bar{v}(x, t) = \sum_{k \in \mathbf{Z}^2 \setminus \{0\}} \bar{v}_k(t) e^{ik \cdot x}.$$

It follows that the smoothing filter (3) in the NS-alpha deconvolution model may be written as

$$\bar{v}_k = D_{N,k} (1 - \alpha^2 |k|^2)^{-1} v_k$$

where

$$D_{N,k} = \sum_{n=0}^N \left(1 - \frac{1}{1 + \alpha^2 |k|^2} \right)^n = \sum_{n=0}^N \left(\frac{\alpha^2 |k|^2}{1 + \alpha^2 |k|^2} \right)^n.$$

Summing the above geometric series yields

$$\frac{D_{N,k}}{1 + \alpha^2 |k|^2} = 1 - \left(\frac{\alpha^2 |k|^2}{1 + \alpha^2 |k|^2} \right)^{N+1}.$$

Observe that

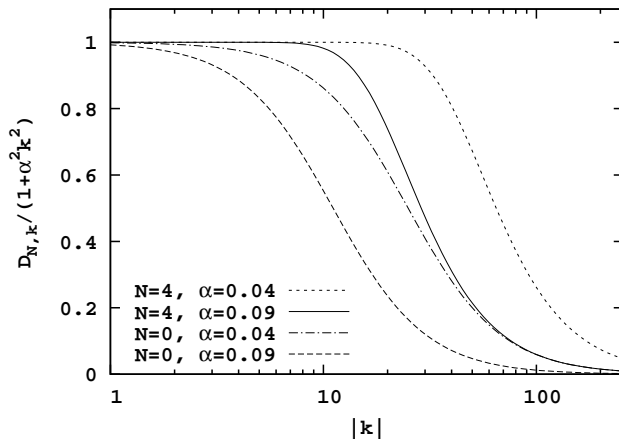
$$\frac{D_{N,k}}{1 + \alpha^2|k|^2} \rightarrow 1 \quad \begin{array}{l} \text{as } N \rightarrow \infty \text{ holding } \alpha \text{ constant,} \\ \text{or as } \alpha \rightarrow 0 \text{ holding } N \text{ constant.} \end{array}$$

At the same time, note that

$$\frac{D_{N,k}}{1 + \alpha^2|k|^2} \rightarrow 0 \quad \text{as } \alpha \rightarrow \infty \text{ holding } N \text{ constant.}$$

The above limits suggest there may be a tradeoff between α and N which could be used to identify an effective averaging length scale α_0 that depends on N .

Figure 1: The smoothing filter in the NS-alpha deconvolution model in Fourier space for four different choices of N and α .



Evidence of such a tradeoff is presented in Figure 1 where four representative curves of the smoothing filter $D_{N,k}/(1 + \alpha^2|k|^2)$ are plotted for N and α where $N \in \{0, 4\}$ and $\alpha \in \{0.04, 0.09\}$. Smaller values of α lead to a smoothing filter which is closer to 1 while larger values of N also yield a filter which is closer to 1. Moreover, the high-frequency attenuation is nearly the same when $N = 4$ and $\alpha = 0.09$ as it is when $N = 0$ and $\alpha = 0.04$. This suggests a clear tradeoff between N and α for which the microscales are the same.

We now perform an asymptotic analysis of $D_{N,k}/(1 + \alpha^2|k|^2)$ as $k \rightarrow \infty$ to precisely identify the effective averaging length scale α_0 that leaves the high-frequency attenuation of the smoothing filter unchanged as N is varied. Since

$$\frac{D_{N,k}}{1 + \alpha^2|k|^2} = 1 - \left(\frac{\alpha^2|k|^2}{1 + \alpha^2|k|^2} \right)^{N+1} \sim \frac{N+1}{\alpha^2|k|^2} \quad \text{as } k \rightarrow \infty,$$

one can rescale the filter by setting $\alpha = \alpha_0\sqrt{N+1}$ where α_0 is constant to obtain an asymptotic decay that is independent of N when $k \rightarrow \infty$. The fact

that $0.09 \approx 0.04\sqrt{4+1}$ now explains why the high-frequency attenuation was nearly the same for two of the curves in Figure 1.

The above identification motivates the definition of the rescaled smoothing filter $H_{N,k}$ in terms of the effective averaging length scale α_0 as

$$H_{N,k} = \frac{1}{1 + (N+1)\alpha_0^2|k|^2} \left\{ 1 - \left(\frac{(N+1)\alpha_0^2|k|^2}{1 + (N+1)\alpha_0^2|k|^2} \right)^{N+1} \right\}.$$

The limit $N \rightarrow \infty$ holding α_0 constant now leads to the non-trivial limit filter

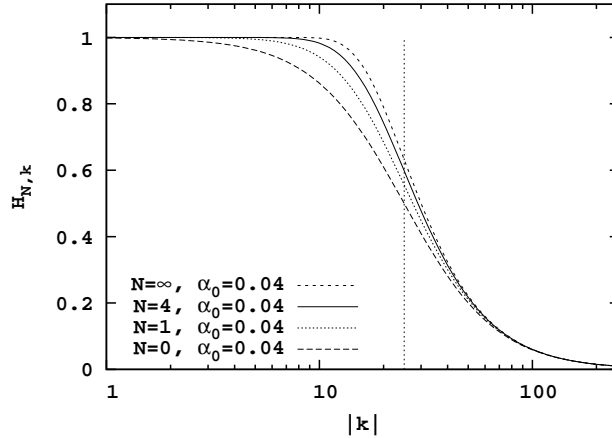
$$H_{\infty,k} = \lim_{N \rightarrow \infty} \frac{D_{N,k}}{1 + (N+1)\alpha_0^2|k|^2} = 1 - \exp\left(\frac{-1}{\alpha_0^2|k|^2}\right).$$

Moreover, for every $N \in \mathbf{N} \cup \{\infty\}$ we have that

$$H_{N,k} \sim \frac{1}{\alpha_0^2|k|^2} \quad \text{as} \quad k \rightarrow \infty$$

and therefore the high-frequency attenuation of this family of filters is independent of N . Figure 2 demonstrates how changing N affects $H_{N,k}$ in the low modes without affecting the microscales.

Figure 2: When α_0 is fixed the cutoff for the high modes is independent of N . The vertical line denotes the wavenumber $|k| = 1/\alpha_0$.



We remark that this is the first time the exponential filter $H_{\infty,k}$ has been derived and proposed for use in the context of turbulence modeling. A Gaussian filter of the form $\exp(-\alpha_0^2|k|^2)$ was considered for the Leray and LANS-alpha models by Geurts and Holm [14]. That filter is a mirror image reflection of the one derived here: Instead of preserving the cutoff in the high modes, it holds fixed the $N = 0$ order of the low modes.

For smooth functions u the filters $H_{N,k}$ have a consistency error given by

$$u - H_{N,k}u = \begin{cases} \mathcal{O}(\alpha_0^{2N+2}) & \text{for } N \in \mathbf{N} \\ \mathcal{O}(\exp(-1/\lambda_0\alpha_0^2)) & \text{for } N = \infty \end{cases} \quad \text{as} \quad \alpha_0 \rightarrow 0$$

where λ_0 is the smallest eigenvalue of the Stokes operator. Therefore, the consistency error as a function of the effective averaging length scale α_0 is the same as the results proved by Stolz, Adams and Kleiser [25], see also Dunca and Epshteyn [10], for the NS-alpha deconvolution model. Moreover, the exponential filter obtained in the limit when $N \rightarrow \infty$ has exponentially small consistency error as $\alpha_0 \rightarrow 0$. We turn now to our computational results.

3 Numerical Methods

The vorticity formulations of the Navier–Stokes equations and the turbulence models described in the introduction are particularly simple in two dimensions. Using the notation $\text{curl } u = \partial u_2 / \partial x_1 - \partial u_1 / \partial x_2$, the two-dimensional incompressible Navier–Stokes equations can be expressed as the scalar equation

$$\frac{\partial \omega}{\partial t} - \nu \Delta \omega + u \cdot \nabla \omega = g \quad \text{where} \quad \omega = \text{curl } u \quad (6)$$

and $g = \text{curl } f$. Similarly, the alpha turbulence models are all given by

$$\frac{\partial m}{\partial t} - \nu \Delta m + \bar{v} \cdot \nabla m = g \quad \text{where} \quad H_N m = \text{curl } \bar{v} \quad (7)$$

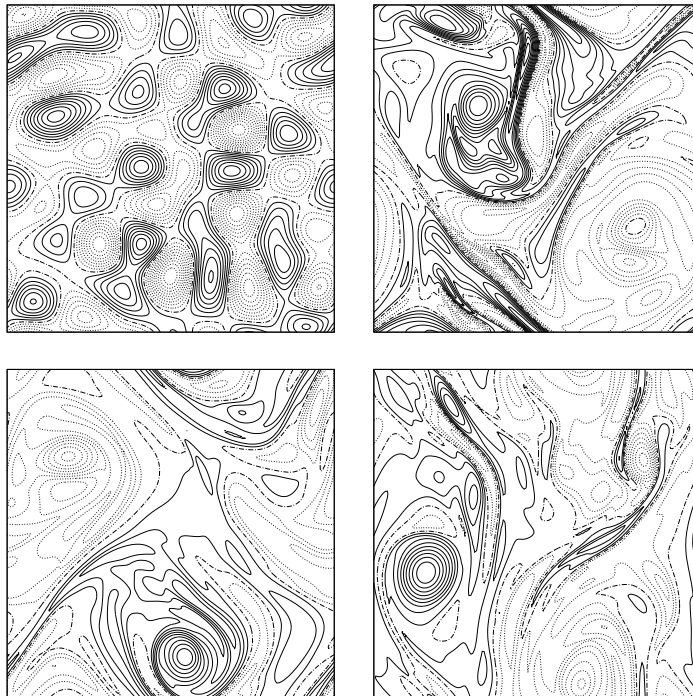
where H_N is the differential operator corresponding to the symbol $H_{N,k}$ in the previous section. We recall equations (7) reduce to the LANS-alpha model when $N = 0$ and that the new exponential-alpha model is obtained when $N = \infty$.

It is well known, see for example Temam [27], that the two-dimensional Navier–Stokes equations are well-posed. That is, these equations possess unique smooth solutions depending continuously on the initial conditions provided the force is sufficiently regular. Foias, Holm and Titi [11] show that three-dimensional LANS-alpha model is also well posed. It follows, trivially, that the two-dimensional LANS-alpha model is well posed. Similar results hold for NS-alpha deconvolution model and also for the new exponential-alpha model.

We shall consider a two-dimensional incompressible flow in a 2π -periodic box forced by a 2π -periodic body force. Specifically, we take $\Omega = [0, 2\pi]^2$, the viscosity $\nu = 0.0001$ and choose a time-independent divergence-free body forcing f supported on the Fourier modes with $16 \leq |k|^2 \leq 34$ such that $\|f\|_{L^2} = 0.0025$ and for which the Grashof number is $G = \nu^{-2} \|f\|_{L^2} = 250\,000$. To obtain such a force, the amplitudes of the Fourier modes were chosen randomly and then rescaled to obtain the desired Grashof number. The exact function used here is depicted top left in Figure 3 and originally appeared in Olson and Titi [22] where it was called f_{25} to indicate its support lied on an annulus about $|k|^2 = 25$ in Fourier space.

Since we have written our fluid equations in vorticity form, it is natural to compute the residual vorticity ρ given by $\rho = \text{curl } R$. No generality is lost in doing this, because we may later recover R by inverting the definition of ρ subject to the condition $\nabla \cdot R = 0$. Note, as the velocity fields present in both

Figure 3: Top left shows the contours of the force $g = \text{curl } f$; in order following are contours of ω at times 25 000, 37 500 and 50 000.



the exact and approximate dynamics are divergence free, so R is divergence free. Therefore, we plug ω into equation (7) to obtain

$$d\rho = ((\bar{u} \cdot \nabla \omega) - (u \cdot \nabla \omega)) dt.$$

Integrating in time then yields

$$\rho(t) = \int_0^t ((\bar{u} \cdot \nabla \omega) - (u \cdot \nabla \omega)) dt. \quad (8)$$

It is worth remarking that at no point does the time evolution of the approximate dynamics (7) governing m enter into the computation of ρ . Indeed, sensitive dependence on initial conditions is well known for the dynamical systems studied here, which in turn, implies there is no shadowing result that could be used to compare separate evolutions of ω and m over long periods of time.

Theoretically the evolution of ω should be determined by the exact dynamics of the two-dimensional incompressible Navier–Stokes equations. As this is not possible in any numerical experiment, we therefore consider as exact the solution ω_k^n to the discrete dynamical system given by the fully-dealiased spectral

Galerkin method for approximating equations (6) in which the linear terms have been integrated exactly in time and the nonlinear term using an Euler method.

Given $K \in \mathbf{N}$ fixed, let

$$\mathcal{K} = \{ (k_1, k_2) \in \mathbf{Z}^2 \setminus \{0\} : -K \leq k_1, k_2 \leq K \}$$

and write

$$\omega^n(x) = \sum_{k \in \mathcal{K}} \omega_k^n e^{ik \cdot x} \quad \text{and} \quad u^n(x) = \sum_{k \in \mathcal{K}} \frac{i(k_2, -k_1)}{|k|^2} \omega_k^n e^{ik \cdot x}.$$

By definition, then, the dynamics of our exact solution are given by

$$\omega^{n+1} = S(\omega^n) \quad \text{for} \quad n = 0, 1, 2, \dots \quad (9)$$

where the discrete semigroup operator S is given by

$$\begin{aligned} S(\omega^n)_k &= \left\{ \omega_k^n - h(u^n \cdot \nabla \omega^n)_k \right\} e^{-\nu|k|^2 h} \\ &+ \frac{2g_k}{\nu|k|^2} e^{-\nu|k|^2 h/2} \sinh(\nu|k|^2 h/2). \end{aligned} \quad (10)$$

Although more accurate and stable time stepping methods could be used, the above is sufficient for our present study. Note that ω_k^n may be viewed as a discrete approximation of the continuous solution ω to equations (6) projected onto the Fourier mode $\exp(ik \cdot x)$ at time $t_n = hn$ for some time step $h > 0$. While S acts on the vorticity, an equivalent semigroup may be defined which acts on the velocity. For notational simplicity we shall refer to both semigroups as S . Thus $u^{n+1} = S u^n$ shall mean $u^{n+1} = \text{curl}^{-1} S \text{curl} u^n$.

We now prove for K fixed and h small enough that the discrete dynamical system (9) possesses a unique global attractor $\mathcal{A}_{K,h}$. This follows directly from following lemma which shows the existence of an absorbing ball. In order to keep track of the dimensional quantities which appear in the proof, define

$$\lambda_0 = \min\{ |k|^2 : k \in \mathcal{K} \} = 1$$

and recall that $g_k = 0$ for $|k|^2 > \lambda_M$ where $\lambda_M = 34$.

Lemma 1 *Let*

$$B = c_0 \frac{\|f\|_{L^2}}{\nu \lambda_0^{1/2}} \quad \text{where} \quad c_0 > 6\lambda_M/\lambda_0.$$

Given K fixed and $L > 0$, there is h small enough and N large enough such that $|w^0| < L$ implies $|w^n| < B$ for all $n \geq N$.

Proof. From (9) we have

$$\omega_k^{n+1} e^{\nu|k|^2 h} = \omega_k^n - h(u^n \cdot \nabla \omega^n)_k + \frac{2g_k}{\nu|k|^2} (e^{\nu|k|^2 h} - 1).$$

Therefore

$$\sum_{k \in \mathcal{K}} \omega_k^{n+1} e^{\nu|k|^2 h} e^{ik \cdot x} = \omega^n - h(u^n \cdot \nabla \omega^n) + \sum_{k \in \mathcal{K}} \frac{2g_k}{\nu|k|^2} (e^{\nu|k|^2 h} - 1) e^{ik \cdot x}.$$

Let

$$|\omega^n|^2 = \|\omega^n\|_{L^2}^2 = 4\pi^2 \sum_{k \in \mathcal{K}} |\omega_k^n|^2.$$

Since all norms are equivalent in finite dimensional spaces, there exists C_K such that $|u^n \cdot \nabla \omega^n|^2 \leq C_K |\omega^n|^4$. Moreover, since $(u^n \cdot \nabla \omega^n, \omega^n) = 0$, then

$$|\omega^n - h(u^n \cdot \nabla \omega^n)|^2 = |\omega^n|^2 + h^2 |u^n \cdot \nabla \omega^n|^2 \leq |\omega^n|^2 (1 + C_K h^2 |\omega^n|^2).$$

For h such that $\nu \lambda_M h < 1$ we have $e^{\nu \lambda_M h} < 3$. It follows that

$$\begin{aligned} \left| \sum_{k \in \mathcal{K}} \frac{2g_k}{\nu|k|^2} (e^{\nu|k|^2 h} - 1) e^{ik \cdot x} \right| &= \left(4\pi^2 \sum_{k \in \mathcal{K}} \frac{4|g_k|^2}{\nu^2|k|^4} (e^{\nu|k|^2 h} - 1)^2 \right)^{1/2} \\ &\leq (e^{\nu \lambda_M h} - 1) \frac{2|f|}{\nu \lambda_0^{1/2}} \leq \nu \lambda_M h \frac{6|f|}{\nu \lambda_0^{1/2}}. \end{aligned}$$

Therefore,

$$\begin{aligned} |\omega^{n+1}|^2 e^{2\nu \lambda_0 h} &\leq |\omega^n|^2 (1 + C_K h^2 |\omega^n|^2) \\ &\quad + 2|\omega^n| (1 + C_K h^2 |\omega^n|^2)^{1/2} \nu \lambda_M h \frac{6|f|}{\nu \lambda_0^{1/2}} \\ &\quad + \nu^2 \lambda_M^2 h^2 \frac{36|f|^2}{\nu^2 \lambda_0} \\ &\leq |\omega^n|^2 (1 + C_K h^2 |\omega^n|^2) (1 + \nu \lambda_0 h) \\ &\quad + \left(\frac{\lambda_M}{\lambda_0} + \nu \lambda_M h \right) \nu \lambda_M h \frac{36|f|^2}{\nu^2 \lambda_0}. \end{aligned}$$

Now, if $B \leq |\omega^n| \leq L$, then

$$|\omega^{n+1}|^2 \leq \alpha(h) e^{-2\nu \lambda_0 h} |\omega^n|^2$$

where

$$\alpha(h) = (1 + C_K h^2 L^2) (1 + \nu \lambda_0 h) + 36 \left(\frac{\lambda_M}{\lambda_0} + \nu \lambda_M h \right) \frac{\nu \lambda_M h}{c_0^2}.$$

Since $\alpha(h) \rightarrow 1$ as $h \rightarrow 0$ and

$$\alpha'(0) = \nu \lambda_0 + 36 \frac{\nu \lambda_M^2}{c_0^2 \lambda_0} < 2\nu \lambda_0,$$

there is h small enough that $\gamma = \alpha(h) e^{-2\nu \lambda_0 h} < 1$ as well as $\nu \lambda_M h < 1$. Let N be large enough that $L \gamma^N < B$. Since $|\omega^n| < B$ implies $|\omega^{n+1}|^2 \leq \gamma B^2 < B^2$,

once $|\omega^n|$ falls below B it stays below B . It follows that $|\omega^{n+1}| < B$ for all $n \geq N$, which completes the proof of the lemma. ■

We remark that, up to the constant c_0 , the bound on B given above is the same as the usual estimate on the absorbing ball of the two-dimensional incompressible Navier–Stokes equations (6), see, for example [27]. Note also that the estimate on the size of h depends on C_K , which we have not explicitly computed here. Lemma 1 is important theoretically; however, as with other *a priori* estimates of this type, the resulting bounds on h and B differ by many orders of magnitude from those suggested by the numerics.

We turn now to the computation of the discrete residual. Project (8) onto the Fourier modes to obtain

$$\rho_k(t_n) = \int_0^{t_n} ((\bar{u} \cdot \nabla \omega)_k - (u \cdot \nabla \omega)_k) dt$$

This integral can be estimated using any of a number of numerical quadratures. For simplicity we define ρ_k^n as the approximation of $\rho_k(t_n)$ given by the Riemann–Stieltjes sum using the left end points of each subinterval. Thus,

$$\rho_k^{n+1} = \rho_k^n + h((\bar{u}^n \cdot \nabla w^n)_k - (u^n \cdot \nabla w^n)_k) \quad (11)$$

where $\rho^0 = 0$ and

$$\bar{u}^n = \sum_{k \in \mathcal{K}} F_{N,k} \frac{i(k_2, -k_1)}{|k|^2} \omega_k^n.$$

As in the continuous case, the discrete residual velocity may be obtained from the residual vorticity. In particular, $R_k^n = i\rho_k^n(k_2, -k_1)/|k|^2$.

Note that R_k^n reflects the modeling error made when replacing our fully discrete dynamical system by a similarly discretized alpha model. It is also possible to track the residual error present in a particular discretization of a continuous dynamical system. For work along these lines please see Banks, Hittinger, Connors and Woodward [1] and references therein. While it may be possible that similar techniques could be used to relate the discrete residuals R_k^n that we compute here to the model error present in the fully-continuous alpha models, we do not pursue this direction of inquiry at the present time.

The computations which appear in this paper were implemented using the MIT/Intel Cilkplus parallel processing extensions to the C programming language and compiled using GCC version 5.1. The fast Fourier transforms used to compute the non-linear term were performed using the FFTW3 software library. All computations were carried out using IEEE 754 double-precision floating point on the PDE Wulf cluster and the UNR Grid at the University of Nevada Reno. The final computations presented here took a total of 2016 core-hours of processing time using Intel Xeon E5-2650 CPUs. The Navier–Stokes solver described in [22] was used to verify the correctness of our computations.

The specific discretization considered here uses a 256×256 spatial grid with $K = 85$ and a time step of $h = 25/4096$. For practical reasons h has been taken to be many orders of magnitude larger than the bounds given in

Lemma 1. Numerically, this choice of parameters leads to a stable numerical scheme with a Courant–Friedrichs–Lewy condition number of

$$\text{CFL} = \frac{Kh}{2\pi} \sup \{|u^n(x_{ij})|_1 : x_{ij} \in \Omega \text{ and } t_n \leq 100\,000\} \approx 0.18$$

where $x_{ij} = 2\pi(i, j)/256$ and $|(u_1, u_2)|_1 = |u_1| + |u_2|$. We henceforth assume that (9) possesses a global attractor $\mathcal{A}_{K,h}$ suitable for our study. Starting from the initial condition $u^0(x) = 0$, we obtain by time $t = 25\,000$ a solution whose statistical properties appear to have reached a steady state.

To further characterize the time scales in our computation, we estimate the eddy turnover time τ using the definition of Gescho, Olson and Titi [13] as

$$\tau = 4\pi^2 \sum_{r=1}^{\infty} r^{-1} E(r) / \left(\sum_{r=1}^{\infty} E(r) \right)^{3/2} \approx 92.05,$$

where $E(r)$, see Figure 4, is the time-averaged energy spectrum given by

$$E(r) = \frac{4\pi^2}{T - T_0} \int_{T_0}^T \sum_{k \in \mathcal{J}_r} |u_k(t)|^2 dt$$

averaged from $T_0 = 25\,000$ to $T = 100\,000$ where

$$\mathcal{J}_r = \{k \in \mathbf{Z}^2 : r - 0.5 < |k| \leq r + 0.5\}.$$

Note that the flow undergoes an additional 814 eddy turnovers on this time interval. We presume, therefore, that u^n lies very near the global attractor of our discrete dynamical system for $t_n \geq 100\,000$. We now describe the discrete ensemble averages that will be used to compute the root-mean-squared residual error in our discrete alpha models.

The discrete ensemble averages may be defined as follows. Let \mathcal{U} be a finite subset of $\mathcal{A}_{K,h}$. For each $u_0 \in \mathcal{U}$ let $R_k^n(u_0)$ be the residual obtained by plugging the solution u_k^n with $u^0 = u_0$ into (11). Take μ in (5) to be the uniform probability measure supported on \mathcal{U} . It follows that

$$\mathcal{E}_{\text{rms}}^n = \langle \|R^n\|^2 \rangle^{1/2} = \left\{ \frac{4\pi^2}{|\mathcal{U}|} \sum_{u_0 \in \mathcal{U}} \sum_{k \in \mathcal{K}} |k|^2 |R_k^n(u_0)|^2 \right\}^{1/2} \quad (12)$$

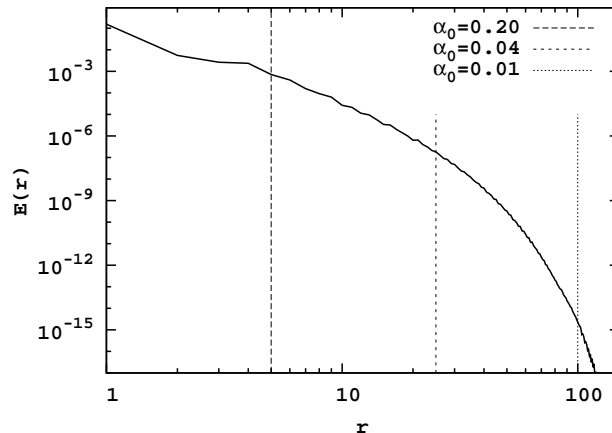
where $|\mathcal{U}|$ denotes the cardinality of \mathcal{U} . Characterizing how $\mathcal{E}_{\text{rms}}^n$ depends on t_n will be the main focus of the computational results in the next section.

4 Computational Results

While domains with periodic boundary conditions are obviously homogeneous, the presence of any non-zero forcing function has the potential to render the statistics of the resulting flow inhomogeneous. As noted by Kurien, Aivalis and

Sreenivasan [24], see also Taylor, Kurien and Eyink [26], even when the body forcing is zero, turbulent flows in periodic domains can possess a certain degree of anisotropy. Referring again to Figure 3, we observe that the forcing function has no regular patterns and that the resulting flow is undergoing complex time dependent behavior that in no way resembles the force. It is hoped, therefore, that the homogeneity and isotropy assumptions made in the derivation of the LANS-alpha and NS-alpha deconvolution models are well enough satisfied that these turbulence models apply to the flow conditions studied here.

Figure 4: The average energy spectrum of u in relation to the wavenumbers $|k| = 1/\alpha_0$ corresponding to three choices of α_0 .



For our numerical study, we compute the root-mean-squared residual error for nine different turbulence models, determined by taking N and α_0 such that $N \in \{0, 4, \infty\}$ and $\alpha_0 \in \{0.01, 0.04, 0.20\}$. Intuitively, for small values of α_0 we expect an alpha model to function as a subgrid-scale model [6, 18] and for large values of α_0 as a Reynolds stress closure [3, 4, 5]. To see how the different values of α_0 considered in our numerical experiments compare with the energetics of a typical flow on the global attractor of (9), Figure 4 plots the energy spectrum $E(r)$ of the solution u^n with initial condition $u^0 = 0$ averaged between times $T_0 = 25\,000$ and $T = 100\,000$ against the vertical lines $|k| = 1/\alpha_0$. Each of these vertical lines represent the wavenumber at which the Fourier modes are attenuated by 50 percent in the smoothing filter of the original LANS-alpha model. As previously illustrated in Figure 2, larger values of N lead to slightly less attenuation at this wavenumber. We remark that the smallest averaging length scale $\alpha_0 = 0.01$ leads to smoothing filters affecting modes in the dissipation range of the energy spectrum, that $\alpha_0 = 0.04$ also affects modes in the inertial range and that the relatively large value of $\alpha_0 = 0.2$ affects all the modes including those in the forcing range and inverse cascade.

The ensemble averages employed for finding the residual error consist of seven independent trajectories. Each trajectory was obtained by first choosing

a random velocity field and then evolving that field forward $T = 100\,000$ units in time, which is far enough to define a point in \mathcal{U} close to the global attractor. While any statistically independent way of choosing the initial random velocity fields could be used, in practice it worked well to choose the Fourier modes of the random velocity field according to a Gaussian distribution in such a way that the expected value of the energy spectrum was the same as the average energy spectrum $E(r)$ shown in Figure 4.

In particular, let $X_{j,k}$ and $Y_{j,k}$ be independent standard Gaussian random variables for $j = 1, \dots, 7$ and $k \in \mathcal{K}$. Now for each j define

$$U_j(x) = \sum_{k \in \mathcal{K}} \frac{i(k_2, -k_1)}{|k|^2} (Z_k + \overline{Z_{-k}}) e^{ik \cdot x}$$

where

$$Z_k = \frac{|k|}{2\pi} \left(\frac{E(r)}{|\mathcal{J}_r|} \right)^{1/2} \left(\frac{X_{j,k} + iY_{j,k}}{2} \right),$$

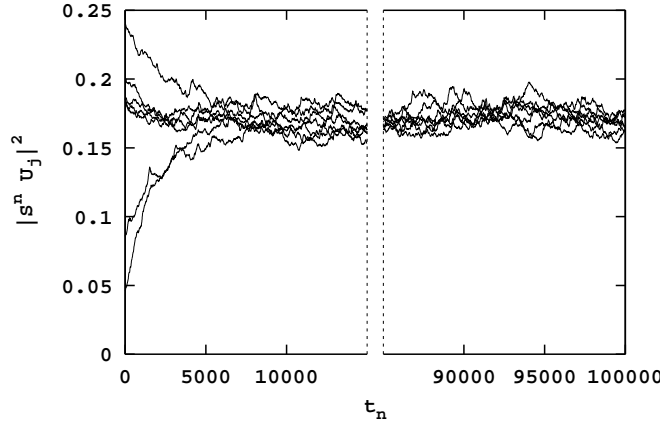
$k \in \mathcal{J}_r$ and $E(r)$ is the time averaged spectrum given in Figure 4. Since

$$\mathbf{E}[|Z_k + \overline{Z_{-k}}|^2] = \frac{|k|^2 E(r)}{16\pi^2 |\mathcal{J}_r|} \mathbf{E}[|X_{j,k} + X_{j,-k}|^2 + |Y_{j,k} - Y_{j,-k}|^2] = \frac{|k|^2 E(r)}{4\pi^2 |\mathcal{J}_r|},$$

then

$$\mathbf{E}[\|U_j\|_{L^2}^2] = 4\pi^2 \sum_{k \in \mathcal{K}} \frac{1}{|k|^2} \mathbf{E}[|Z_k + \overline{Z_{-k}}|^2] = \sum_{r=1}^{\infty} E(r).$$

Figure 5: Evolution of seven independent choices for U_j on $[0, 100\,000]$ leading to the points in \mathcal{U} . Note that the graph has been broken and data omitted between times $t_n = 15\,000$ and $t_n = 85\,000$.



Although U_j has been constructed to have an expected energy spectrum similar to a point on the attractor $\mathcal{A}_{K,h}$ of (9), it is unlikely that $U_j \in \mathcal{A}_{K,h}$

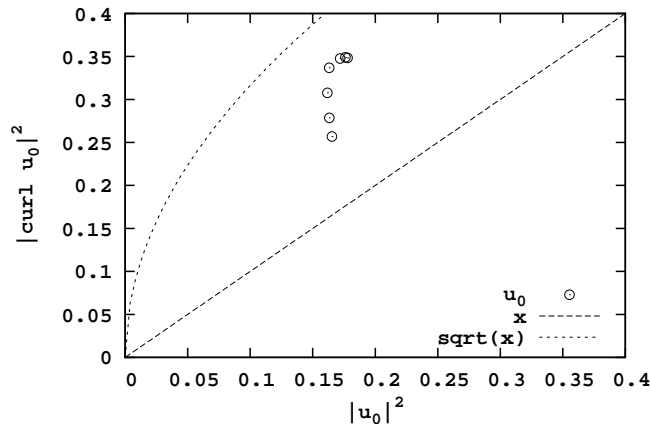
or even that U_j is very near the attractor. Therefore, we evolve each U_j forward sufficiently far in time to obtain a point sufficiently close to $\mathcal{A}_{K,h}$. It is these points which will comprise the set \mathcal{U} used for the ensemble average (12). Specifically, we take

$$\mathcal{U} = \{S^N U_j : j = 1, \dots, 7\}$$

where $N = T/h$ and $T = 100\,000$.

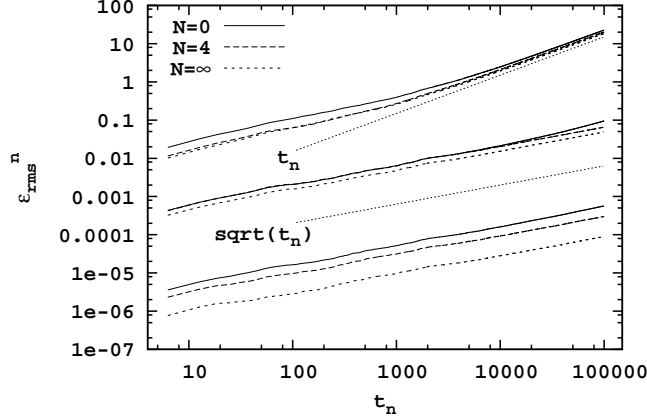
Figure 5 shows the evolution of $\|S^n U_j\|_{L^2}^2$ for $j = 1, 2, \dots, 7$. Note that the statistical properties of the energy appear to have reached a steady state by $t_n = 25\,000$ and by time $t_n = 100\,000$ each flow has undergone approximately 1000 large-eddy turnovers. We presume, for the same reasons as before, that each element of \mathcal{U} is near the discrete global attractor $\mathcal{A}_{K,h}$. This presumption is further supported by Figure 6 which plots the points $u_0 \in \mathcal{U}$ used for our ensemble averages in the energy-ensrophy plane. The fact that all seven points lie between the parabola and the line is consistent with the analysis of Dascaluic, Foias and Jolly [8] on the location of the global attractor for the two-dimensional incompressible Navier–Stokes equations.

Figure 6: Locations in the energy-ensrophy plane of the seven independent points $u_0 \in \mathcal{U}$ used for the ensemble averages.



Curves showing the evolution of the ensemble-averaged root-mean-squared residual error $\mathcal{E}_{\text{rms}}^n$ for $N \in \{0, 4, \infty\}$ and $\alpha_0 \in \{0.01, 0.04, 0.20\}$ are plotted in Figure 7. For $\alpha_0 = 0.20$ the residual error is the largest and grows linearly when $t_n \geq 4000$ for each value of N . For $\alpha_0 = 0.04$ the curves group together in the middle of the graph and grow as $\sqrt{t_n}$. In this group the curve corresponding to $N = 0$ deviates from the other two when $t_n \geq 20000$ and starts to grow at a slightly faster rate. This deviation, though slight in the log-log plot, is significant as our further analysis indicates. For $\alpha_0 = 0.01$ the residual error is the least and separate curves appear at bottom of the graph for the different values of N . Each of these curves grow as $\sqrt{t_n}$ over the entire range.

Figure 7: Evolution of $\mathcal{E}_{\text{rms}}^n$ for nine different choices of parameters. The top three curves correspond to $\alpha_0 = 0.20$, the middle three to $\alpha_0 = 0.04$ and the bottom three to $\alpha_0 = 0.01$. Values for N are as indicated.



Under the assumption that the residual error is of the form (4), we compute the most-likely values of $\text{Tr } Q$ and $\|F_b\|^2$ as

$$\widehat{\text{Tr } Q} = C_2 \quad \text{and} \quad \|\widehat{F}_b\|^2 = C_2$$

where C_1 and C_2 are the least squares fit to $(\mathcal{E}_{\text{rms}}^n)^2 \approx C_2 t^2 + C_1 t$. The relative size of the systematic bias versus the stochastic error at the end of each computational run is given by the quotient $\eta = C_2 T / C_1$ where $T = 100\,000$.

Table 1: Least squares estimates of $\widehat{\text{Tr } Q}$ and $\|\widehat{F}_b\|^2$ for different choices of α_0 and N . The last column indicates the relative size η of the systematic bias versus the stochastic error at time $T = 100\,000$.

α_0	N	$\widehat{\text{Tr } Q}$	$\ \widehat{F}_b\ ^2$	η
0.01	0	2.588×10^{-12}	6.364×10^{-18}	0.25
0.01	4	8.704×10^{-13}	2.843×10^{-19}	0.00
0.01	∞	7.745×10^{-14}	3.016×10^{-20}	0.04
0.04	0	4.164×10^{-08}	4.858×10^{-13}	1.17
0.04	4	4.192×10^{-08}	6.952×10^{-15}	0.02
0.04	∞	2.374×10^{-08}	-3.286×10^{-16}	-0.00
0.20	0	1.348×10^{-04}	4.984×10^{-08}	36.97
0.20	4	5.166×10^{-05}	3.983×10^{-08}	77.10
0.20	∞	5.353×10^{-05}	3.346×10^{-08}	62.52

Table 1 reports the values of $\widehat{\text{Tr } Q}$, $\|\widehat{F}_b\|^2$ and η for the computational runs

given in Figure 7. Note that when α_0 is fixed, the estimates of $\text{Tr } Q$ have similar magnitudes for the different values of N . Moreover, the estimates of $\|F_b\|$ are nearly the same when $N = 4$ or $N = \infty$. For the choice of parameters $\alpha_0 = 0.04$ and $N = \infty$ the estimated value of $\|F_b\|^2$ is negative, which is clearly non-physical. While more powerful methods of parameter estimation could avoid such impossibilities, in this case such a result indicates that the systematic bias is essentially zero. A more detailed study of the residual error, in which the distribution of an assumed Q -Brownian motion is solved for *a posteriori* as in [16], is left for future work.

The similarity between the results in Table 1 for $N = 4$ and $N = \infty$ is consistent with [25] wherein it is reported that for all tested applications $N = 3$ already gives acceptable results, and that choosing N larger than 5 does not improve the results significantly. The value $\alpha_0 = 0.20$ leads to $\eta \gg 1$ for every choice of N , which suggests systematic bias dominates the residual error when α_0 is large. On the other hand, the value $\alpha_0 = 0.01$ leads to $\eta \ll 1$ for every choice of N as does the value $\alpha = 0.04$ for $N = 4$ and $N = \infty$. In these cases, the systematic bias is negligible over a time period of more than 1000 large eddy turnovers. We conclude the residual error behaves as if the model error were given by stochastic force. This is the main computational result that was referred to in the introduction of this paper.

We end by following up on the observation that the time evolution of the residual error when $\alpha_0 = 0.04$ and $N = 0$ deviated slightly from the line $\sqrt{t_n}$ in Figure 7. For this choice of parameters Table 1 indicates that $\eta \approx 1.17$. This means that by the end of the computational run what appears to be systematic bias contributes more than 50 percent to the total residual error. Thus, the model error in the original LANS-alpha has significant bias when $\alpha_0 = 0.04$.

5 Conclusions

During our study of the model error in the LANS-alpha and NS-alpha deconvolution modules of turbulence we identified an effective averaging length scale $\alpha_0 = \alpha/\sqrt{N+1}$ and created a new turbulence model, the exponential-alpha model, corresponding to the limit as $N \rightarrow \infty$. We also developed a computational method for studying the model error by calculating the time evolution of the root-mean-squared residual error taken over an ensemble of trajectories on the global attractor. Numerical computation then showed that

- if $\alpha_0 = 0.01$ or if $\alpha_0 = 0.04$ and $N \in \{4, \infty\}$, then $\mathcal{E}_{\text{rms}}^n$ grows as $\sqrt{t_n}$;
- if $\alpha_0 = 0.20$ or if $\alpha_0 = 0.04$ and $N = 0$, then $\mathcal{E}_{\text{rms}}^n$ grows linearly as t_n ,

for a particular time dependent forcing function supported on the Fourier modes $16 \leq |k|^2 \leq 34$ with Grashof number $G = 250\,000$. Thus, when α_0 is sufficiently small, the model error in the LANS-alpha and NS-alpha deconvolution models behaves as a stochastic force; however, when α_0 is too large, the model error

includes systematic bias. Our results also show that the NS-alpha deconvolution model of order $N = 4$ performs similarly to the exponential-alpha model.

We emphasize that the method of computing the model error employed in this paper avoids the difficulty that there is no shadowing result which can be used to compare separate evolutions of approximate dynamics to exact dynamics over long periods of time. For the alpha models studied here, our identification of α_0 allows direct comparison of the residual error while holding the behavior in the microscales essentially constant.

Preliminary results indicate that the systematic bias in the $\alpha_0 = 0.20$ case is concentrated on the modes present in the forcing function. It is possible this systematic bias indicates that the flow given by the exact dynamics was not fully homogeneous as assumed when deriving the various alpha models. In general, the growth characteristics of $\mathcal{E}_{\text{rms}}^n$ could be used to compare the performance of other turbulence models and the validity of the assumptions under which those models were derived. Future work is planned to study the analytic properties of the new exponential alpha model proposed in this paper, to use the effective averaging length scale α_0 to compare subgrid scale models for flows with more complicated boundary conditions, to study how the homogeneity and isotropy of the exact flow depend on the body forcing and to further characterize the statistical properties of the residual error.

Acknowledgements

The author was supported in part by NSF grant DMS-1418928.

References

- [1] J. Banks, J. Hittinger, J. Connors, C. Woodward, A posteriori error estimation via nonlinear error transport with application to shallow water. *Recent advances in scientific computing and applications*, Contemp. Math., vol. 586, Amer. Math. Soc., 2013, pp. 35–42,
- [2] Y. Cao, E.S. Titi, On the rate of convergence of the two-dimensional α -models of turbulence to the Navier–Stokes equations. *Numer. Funct. Anal. Optim.*, vol. 30, no. 11–12, 2009, pp. 1231–1271.
- [3] S. Chen, C. Foias, D.D. Holm, E. Olson, E.S. Titi, S. Wynne, The Camassa–Holm equations as a closure model for turbulent channel and pipe flow, *Phys. Rev. Lett.*, vol. 81, 1998, pp. 5338–5341.
- [4] S. Chen, C. Foias, D.D. Holm, E. Olson, E.S. Titi, S. Wynne, A connection between the Camassa–Holm equations and turbulent flows in pipes and channels, *Phys. Fluids.*, vol. 11, 1999, pp. 2342–2353.
- [5] S. Chen, C. Foias, D.D. Holm, E. Olson, E.S. Titi, S. Wynne, The Camassa–Holm equations and turbulence, *Physica D*, vol. 133, 1999, pp. 49–65.

- [6] S. Chen, D.D. Holm, L.G. Margolin, R. Zhang, Direct numerical simulations of the Navier–Stokes alpha model, *Physica D*, vol. 133, 1999, pp. 66–83.
- [7] A. Cheskidov, Boundary layer for the Navier–Stokes-alpha model of fluid turbulence. *Arch. Ration. Mech. Anal.*, vol. 172, no. 3, 2004, pp. 333–362.
- [8] R. Dascaliuc, C. Foias, M.S. Jolly, Relations between energy and enstrophy on the global attractor of the 2-D Navier–Stokes equations, *J. Dynam. Differential Equations*, vol 17, no. 4, 2005, pp. 643–736.
- [9] G. Deugoué, P.A. Razafimandimby, Mamadou Sango, On the 3-D stochastic magnetohydrodynamic- α model. *Stochastic Process. Appl.*, vol. 122, no. 5, 2012, pp. 2211–2248.
- [10] A. Dunca, Y. Epshteyn, On the Stolz–Adams deconvolution model for the large-eddy simulation of turbulent flows, *SIAM J. Math. Anal.*, vol. 37, no. 6, 2006, pp. 1890–1902.
- [11] C. Foias, D.D. Holm, E.S. Titi, The Navier–Stokes-alpha model of fluid turbulence, *Physica D*, vol. 152, 2001, pp. 505–519.
- [12] C. Foias, D.D. Holm, E.S. Titi, The three dimensional viscous Camassa–Holm Equations and their relation to the Navier–Stokes equations and turbulence theory, *Journal of Dynamics and Differential Equations*, vol. 14, 2002, pp. 1–35.
- [13] M. Gesho, E. Olson, E.S. Titi, A Computational Study of a Data Assimilation Algorithm for the Two-dimensional Navier–Stokes Equations, submitted, arXiv:1505.01234.
- [14] B.J. Geurts, D.D. Holm, Leray and LANS- α modelling of turbulent mixing, *J. Turbul.*, vol. 7, 2006, pp. 10–33.
- [15] M.W. Hecht, D.D. Holm, M.R. Petersen, B.A. Wingate, The LANS- α and Leray turbulence parameterizations in primitive equation ocean modeling. *J. Phys. A*, vol. 41 no. 34, 2008, pp. 344009–344023.
- [16] V.H. Hoang, K.J.H. Law, A.M. Stuart, Determining white noise forcing from Eulerian observations in the Navier-Stokes equation, *Stoch. Partial Differ. Equ. Anal. Comput.*, vol. 2, no. 2, 2014, pp. 233–261.
- [17] A.A. Ilyin, E.S. Titi, Attractors for the two-dimensional Navier-Stokes- α model: an α -dependence study. *J. Dynam. Differential Equations* 15, no. 4, 2003, pp. 751–778.
- [18] T. Kim, M. Neda, L.G. Rebholz, Eliot Fried, A numerical study of the Navier–Stokes- $\alpha\beta$ model, *Comput. Methods Appl. Mech. Engrg.*, vol. 200, 2011, pp. 2891–2902.

- [19] M.C. Lopes Filho, H.J. Nussenzveig Lopes, E.S. Titi, A. Zang, Convergence of the 2D Euler- α to Euler equations in the Dirichlet case: indifference to boundary layers, *Phys. D* 292/293, 2015, pp. 51–61.
- [20] J.E. Marsden, S. Shkoller, The anisotropic Lagrangian averaged Euler and Navier-Stokes equations, *Arch. Ration. Mech. Anal.* vol. 166, no. 1, 2003, pp. 27–46.
- [21] P.D. Mininni, D.C. Montgomery, A.G. Pouquet, A numerical study of the alpha model for two-dimensional magnetohydrodynamic turbulent flows, *Phys. Fluids*, vol. 17, 2005, pp. 35112–35117.
- [22] E. Olson, E.S. Titi, Determining modes for continuous data assimilation in 2D turbulence. *J. Statist. Phys.*, vol. 113, no. 5-6, 2003, pp. 799–840.
- [23] L.G. Rebholz, A family of new, high order NS- α models arising from helicity correction in Leray turbulence models, *Journal of Mathematical Analysis and Applications*, vol. 342, 2008, pp. 246–254.
- [24] S. Kurien, K. Aivalis and K. Sreenivasan, Anisotropy of small-scale scalar turbulence, *J. Fluid Mech.*, vol. 448, 2001, pp. 279–288.
- [25] S. Stolz, N.A. Adams, and D. Kleiser, An approximate deconvolution model for large-eddy simulation with application to incompressible wall-bounded flows, *Phys. Fluids*, vol. 13, 2001, pp. 997–1015.
- [26] M.A. Taylor, S. Kurien and G.L. Eyink, Recovering isotropic statistics in turbulence simulations: The Kolmogorov 4/5th- Law, *Phys. Rev. E*, vol. 68, 2003, pp. 26–31.
- [27] R. Temam, *Navier–Stokes equations and nonlinear functional analysis*, second edition, CBMS-NSF Regional Conference Series in Applied Mathematics, Vol. 66. Society for Industrial and Applied Mathematics, 1995, pp. 1–141.
- [28] Y. Xiao, Z. Xin, On 3D Lagrangian Navier–Stokes α model with a class of vorticity-slip boundary conditions. *J. Math. Fluid Mech*, vol. 15, no. 2, 2013, pp. 215–247.

